RESEARCH ARTICLE

A Novel Compensation Circuit of the Capacitive Power Transfer System With High Performance of Anti-Misalignment

HUI DENG[1], (Senior Member, IEEE), HUILIN GE[2], AND JING LIAN[3]

[1]Xiongan National Innovation Center Technology Company Ltd., Baoding 071703, China
[2]School of Automation, Jiangsu University of Science and Technology, Zhenjiang 212003, China
[3]School of Automation, Nanjing University of Information Science and Technology, Nanjing 210044, China

Corresponding author: Jing Lian (003594@nuist.edu.cn)

ABSTRACT Capacitive power transfer (CPT) techniques have garnered significant attention in recent years. However, the misalignment of the coupler can lead to variations in the coupling coefficient, which further degrees the reliability of the CPT system and influence the lifetime of loads. In fact, a high-performance CPT system should not only realize nearly input zero phase angle (ZPA), constant output, and soft-switching of MOSFETs, but also exhibit exceptional anti-misalignment performance. Based on the double-sided LC compensation circuit, the LCLC-L compensation circuit with high misalignment tolerance is proposed and systematically analyzed in this paper. The redundant compensation capacitor is removed to reduce the volume of the compensation circuit and an additional L-C circuit is added to regulate the output characteristics of the CPT circuit. The proposed CPT circuit can also realize nearly input ZPA, soft-switching, and constant output. Besides, without complex control strategy, the output current of the proposed CPT circuit can maintain constant even though the distance of the coupler misalignment is large. Finally, the double-sided LC-compensated CPT prototype and the LCLC-L-compensated CPT circuit with the output current of 2 A and the maximum output power of 120 W are built to verify the analysis. Compared to the double-sided LC-compensated CPT circuit. The output current of the proposed CPT circuit is basically unaffected by the coupler misalignment.

INDEX TERMS Capacitive power transfer, LCLC-L compensation, anti-misalignment, soft-switching, load-independent outputs.

I. INTRODUCTION

As one of the main solutions to realize wireless power transfer (WPT), capacitive power transfer (CPT) technique holds significant importance due to its cost-effective, lightweight nature, and absence of eddy-current losses. With advancements in high-frequency switching devices and compensation circuits, CPT can be applied in many fields, such as biomedical implants [1], [2], underwater systems [3], [4] and electric vehicle (EV) charging [5], [6], etc. Consequently, CPT technique exhibits immense market potential and promising

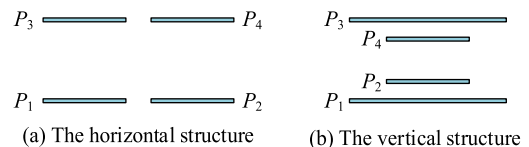The associate editor coordinating the review of this manuscript and approving it for publication was Chun-Hsing Li.

FIGURE 1. The structure of the four-plate capacitive coupler.

development prospects, necessitating further comprehensive research in this domain.

The capacitive coupler of CPT is usually formed by four metal plates and two pairs of plates are horizontally separated as shown in Figure 1(a) [7], [8], [9]. However,

this structure occupies a significant amount of space and results in relatively small leakage capacitances. To elevate the leakage capacitances, external capacitors are added on both the primary and secondary sides of the coupler, which unfortunately increases system bulkiness. In order to minimize installation space while reducing the number of external capacitors required, a compact vertical structure shown in Figure 1(b) is proposed in [10], which has been widely adopted across various applications. Besides, several high-performance compensation circuits, such as the double-sided LCLC compensation circuit [11], the LCL-L compensation circuit [6], and the LC-CLC compensation circuit [12], have been proposed to achieve load-independent output. In order to eliminate reactive power, it is necessary for the input voltage and input current to be in-phase [7], [13], [14]. However, in practical application, the input current slightly lags behind the input voltage to permit a small inductive phase angle for zero voltage switching operation. Previous studies have investigated the complex relationship between input phase angle and normalized parameters under different loading conditions [15], [16]. Additionally, maintaining a constant output current is crucial for satisfying the charging demands of loads in CPT systems [17], [18], [19].

Compared to IPT systems, CPT systems are less sensitive to displacements between the primary plates and the secondary plates. However, in practical operation scenarios where significant misalignment or substantial changes in power transfer distance occur, the equivalent capacitances of the compact vertical capacitive coupler may undergo dramatic variations. Consequently, the CPT system falls out of resonance, directly influencing the output power of the aforementioned CPT systems. In severe cases, the operational safety of the system cannot be guaranteed. A lot of research has been undertaken to improve the anti-misalignment performance of IPT systems. Several high-performance IPT couplers have been introduced and compared in [20] and [21]. A dual-receiver inductive EV charging system with high misalignment tolerance couplers is proposed in [22]. Besides, this IPT system can realize CC and CV output. Furthermore, for dynamic EV charging, a control strategy and efficiency enhancement topology for dual-receiver IPT system are proposed in [23]. The operational mechanism of CPT is similar to that of IPT. Therefore, a comprehensive analysis of IPT can promote the research of CPT. To compensate for the misalignments of the capacitive coupler, a tunable multistage matching network with controllable compensation capacitors is proposed in [20]. Together with a controllable compensation inductor, a matrix charging pad is designed to control the power flow and regulate the output voltage under variable coupling conditions [21]. A capacitive coupler array and a biologically inspired capacitive leaf cell receiver paired with position-independence feature are present in [22]. However, the structure of this novel capacitive couplers is bulky. A high-order compensated capacitive power transfer systems with misalignment insensitive resonance is proposed in [23]. This compensation circuit contains six compensation

components. An active variable reactance rectifier is used in [24] to continuously compensate for misalignments and air gap variations between metal plates, which also increases the size and cost of a system. Without additional components or plates added to a CPT system, a dual-loop control method is proposed in [25] to improve the misalignment tolerance. Other approaches to eliminate the influence of coupling variations on the output power are combining the inductive power transfer (IPT) system and the CPT system to form a hybrid WPT system [26], [27]. Similarly, the complexity of the WPT system increases. Besides, several novel capacitive couplers are proposed to improve misalignment tolerance characteristics [28], [29], [30].

Based on the above analysis, this paper proposes a novel compensation circuit to against coupling variations of CPT systems. Since the output current is adjustable and approximately constant, the proposed CPT system can satisfy the charging demands of different loads. To save installation space, the vertical structure of the four-plate capacitive coupler shown in Figure 1(b) is used in this paper. As analyzed in Section II, only five components are used in the compensation circuit and a complex control strategy is avoided, which makes the CPT system more compact and simpler. The nearly input ZPA is achieved to guaranteed the soft-switching of MOSFETs. And the output current of the proposed CPT basically holds steady even though the coupling varies largely. In Section III, the parameter design procedure of the proposed CPT system is given and the coupling tolerance of the system is analyzed. In Section IV, a CPT prototype is built to verify the proposed compensation circuit and parameter design procedure. Section V concludes the paper.

II. CHARACTERISTIC ANALYSIS OF THE PROPOSED COMPENSATED CIRCUIT

To simplify the analysis, First-Harmonic Approximation (FHA) is used in this paper and the capacitive coupler is equivalent to the Π-type model, which is shown in Figure 2(a) where C_M is the mutual capacitor, C_P is the primary capacitor, and C_S is the secondary capacitor.

(a) The double-sided LC-compensated CPT circuit

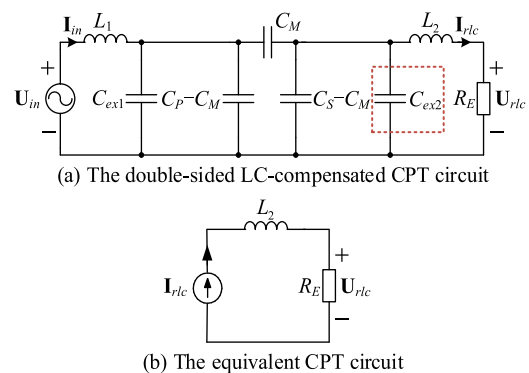(b) The equivalent CPT circuit

FIGURE 2. The equivalent circuits of the double-sided LC-compensated CPT circuit.

The double-sided LC-compensated CPT circuit is suitable for providing power to lithium batteries and it can achieve input zero phase angle (ZPA) and load-desired constant current (CC) output. To facilitate the analysis, as shown in Figure 2(a), the equivalent double-sided LC-compensated CPT system is driven by the voltage $\mathbf{U}_{in}$ and the lithium batteries is equivalent to a load R_E. The compensation circuit is composed by L_1, L_2, C_{ex1}, and C_{ex2}. As shown in Figure 2(b), to realize load-independent CC output, the input voltage $\mathbf{U}_{in}$, compensation inductor L_1, compensation capacitors C_{ex1} and C_{ex2}, and the capacitive coupler are converted to a current source which can provide constant current for the load [27]. Since the permittivity of vacuum is 8.85×10^{-12} F/m, the equivalent capacitances of the capacitive coupler are all in the pF-range which are quite small. To reduce the volume and voltages stresses of the whole system, compensation capacitors C_{ex1} and C_{ex2} are necessary to elevated the equivalent capacitances of the coupler.

Since the function of C_{ex1} is identical with C_{ex2}, to reduce the volume of the CPT circuit in Figure 2(a), compensation capacitor C_{ex2} in red dashed box could be removed. To simplify the analysis, the Π-type model of the capacitive coupler can be converted to the T-type model, which is shown in Figure 3. Defining $C_1 = C_{ex} + C_P$, the T-type model of the capacitive coupler in Figure 3 satisfies

$$C_A = \frac{C_1 C_S - C_M^2}{C_S - C_M}$$
$$C_B = \frac{C_1 C_S - C_M^2}{C_M}$$
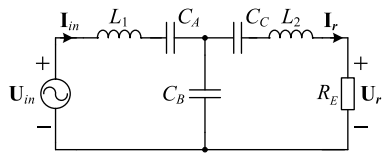$$C_C = \frac{C_1 C_S - C_M^2}{C_1 - C_M} \quad (1)$$

FIGURE 3. The equivalent CPT circuit with T-type model.

Using Kirchhoff current law (KCL) and Kirchhoff voltage law (KVL), the output current of the equivalent circuit shown in Figure 3 can be calculate as

$$\mathbf{I}_{mis} = \frac{t\mathbf{U}_{in}}{1 + (j\omega C_B + t)\left(j\omega L_1 + \frac{1}{j\omega C_A}\right)} \quad (2)$$

where $t = \frac{1}{R_E + j\omega L_2 + \frac{1}{j\omega C_C}}$.

To realize input ZPA and CC output, compensation inductors L_1 and L_2 obey [31]

$$L_1 = \frac{1}{\omega^2}\left(\frac{1}{C_A} + \frac{1}{C_B}\right)$$
$$L_2 = \frac{1}{\omega^2}\left(\frac{1}{C_C} + \frac{1}{C_B}\right) \quad (3)$$

Submitting (3) into (2), the output current is written as

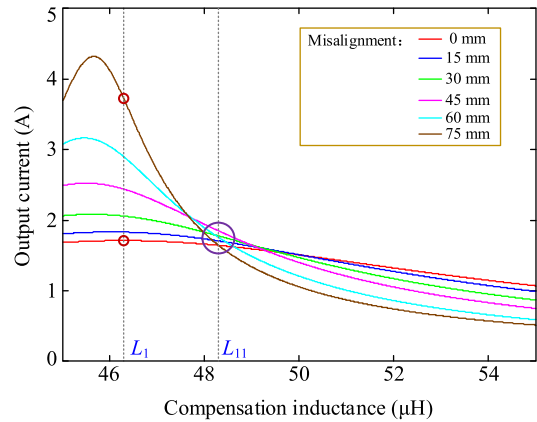$$\mathbf{I}_{rlc} = -j\omega C_B \mathbf{U}_{in} \quad (4)$$

FIGURE 4. Compensation inductances versus the output current.
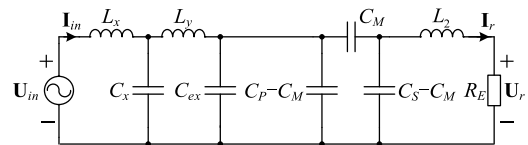

FIGURE 5. The proposed CPT circuit.

The value of the mutual capacitor C_M would decrease when the misalignment of the coupler happens. Consequently, the output current increases sequentially based on equations (1) and (4). As shown in Figure 2(b), L_2 is in series with the equivalent current source, it will not influence the output current and it is used to regulate the phase angle of the input voltage and input current to realize the soft switching. Thus, L_2 cannot be used to reduce the influence of the variation of C_M to the output current. Compensation inductances versus the output current is given in Figure 4. According to Figure 4, if the double-sided LC-compensated CPT circuit operates at its theoretical value, the output current will change dramatically in case of misalignment. As shown in in Figure 4, a slightly increment of L_1 can diminish the variation of the output current even though misalignment happens. Defining the compensation inductance shown in Figure 4 with high anti-misalignment performance be L_{11}, to achieve high tolerance of coupler misalignments and guarantee the nearly input ZPA, the inductor L_1 is replaced with L_x-C_x-L_y circuit and the equivalent inductance at the primary side should be L_{11}. Thus, the CPT circuit in Figure 3 can be converted to the LCLC-L-compensated CPT system in Figure 5 with

$$L_1 = L_x + L_y \quad (5)$$

To facilitate the analysis, Figure 5 can be converted to Figure 6. With the additional L_x-C_x circuit, the input voltage

$\mathbf{U}_{in}$ is converted to $\mathbf{U}_{in1}$ and

$$\mathbf{U}_{in1} = \frac{\mathbf{U}_{in}}{1 - \omega^2 L_x C_x} \qquad (6)$$

According to Figure 4, parameters C_x, L_x, and L_y should be equivalent to the inductance L_{11} and

$$L_{11} = L_1 - L_x + \frac{L_x}{1 - \omega^2 C_x L_x} \qquad (7)$$
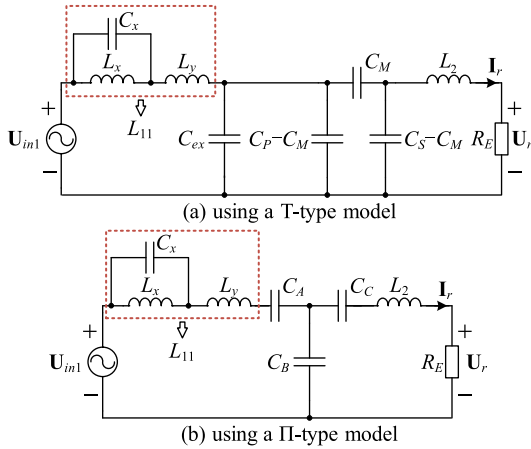

FIGURE 6. The equivalent circuits of Figure 5.

The CPT circuits in Figure 6 are similar with CPT circuits in Figure 2 and Figure 3. Thus, if L_{11} is approximately equal to L_1, with (3), the output current of the proposed CPT circuit is given as

$$\mathbf{I}_r = -j\omega C_B \mathbf{U}_{in1} = -j\omega C_B \frac{\mathbf{U}_{in}}{1 - \omega^2 L_x C_x} \qquad (8)$$

When misalignment happens, equivalent capacitances of the capacitive coupler change, which are denoted by C'_M, C'_P, C'_S, C'_A, C'_B, and C'_C respectively. Since the compensation parameters cannot resonate with the capacitive coupler, the output current of the proposed CPT circuit does not follow (4). Using KCL, the output current of the proposed CPT circuit under the coupler misalignment is calculated as

$$\mathbf{I}_{rmis} = \frac{t_1 \mathbf{U}_{in1}}{1 + (j\omega C'_B + t_1)\left(j\omega L_{11} + \frac{1}{j\omega C'_A}\right)} \qquad (9)$$

where $t_1 = \frac{1}{R_E + j\omega L_2 + \frac{1}{j\omega C'_C}}$.

Equation (9) bears resemblance to (2), suggesting that the output characteristics of the double-sided LC-compensated CPT circuit and the proposed CPT circuit are fundamentally similar. According to Figure 4, a small increase in L_1 can reduce the fluctuation of the output current. As shown in Figure 5 and Figure 6, the compensation inductor at the primary side can be equivalent to L_{11} by adding L_x and C_x. If L_{11} is equivalent to L_1 plus a small increase in L_1 shown in Figure 4, the influence of misalignments on the output current can be reduced. Then the output current of the proposed CPT circuit can be constrained to a specific value, i.e., $\mathbf{I}_r = \mathbf{I}_{rmis}$.

Inductor L_2 is used in some researches to guarantee the soft switching of MOSFETs. With additional L_x-C_x circuit and (3), the input impendence is simplified as

$$Z_{in} = \frac{j\omega^3 C_B^2 (L_{11} - L_1)^2 + L_{11} - L_1}{\omega C_B R_E (L_{11} - L_1) \frac{2I_r - I_{rlc}}{U_{in}} + \frac{j}{\omega}\left(\frac{I_r - I_{rlc}}{I_{rlc}}\right)^2} \qquad (10)$$

With (10), the input impedance can be modulated to be slightly inductive. Then the soft-switching of MOSFETs is realized and the input reactive power of the CPT circuit is significantly reduced.

III. COUPING VARIATIONS ANALYSIS AND SYSTEM DESIGN

A. THE INFLUENCE OF MISALIGNMENTS ON EQUIVALENT CAPACITANCES

The vertical structure of the four-plate capacitive coupler is used in this paper. As given in Figure 1(a), p is the length of square metal plates P_1 and P_3, q is the length of square metal plates P_2 and P_4, d is the air gap between P_1 and P_3, and d_1 is the distance of P_1-P_2 or P_3-P_4. Considering the space limitation, the coupler is designed as $p = 500$ mm and $q = 350$ mm. As illustrated in Figure 7, misalignment between the primary plates and the secondary plates may happen in X-direction, Y-direction, both X- and Y-direction, rotation-direction, or Z-direction. Taking misalignment in X- or Y-direction, $d = 4$ mm, and $d_1 = 3$ mm as an example, equivalent capacitances corresponding to coupler misalignment are shown in Table 1. According to Table 1, with the increase of plate deviation, C_M decreases while $C_P - C_M$ and $C_S - C_M$ increase.
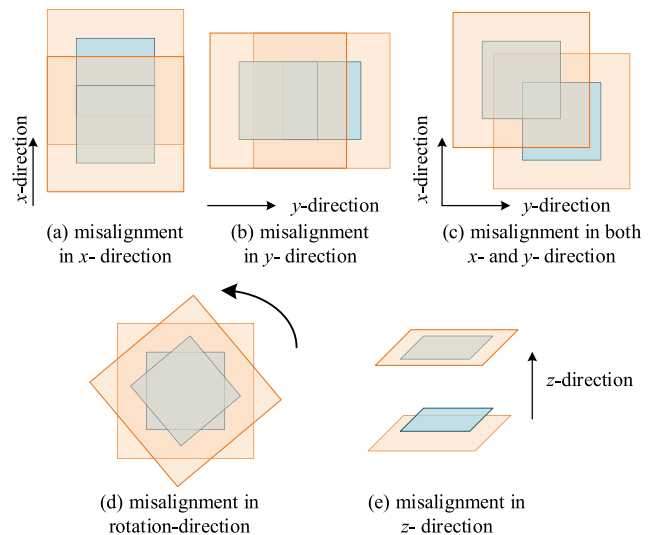

FIGURE 7. The misalignment of a four-plate capacitive coupler.

B. PARAMETER DESIGN PROCEDURE

The proposed CPT system with high misalignment tolerance is given in Figure 8. The DC voltage U_{DC} is converted to a high frequency AC voltage u_{AB}. The fundamental component

TABLE 1. Misalignments in X- or Y-direction and their and their corresponding equivalent capacitances.

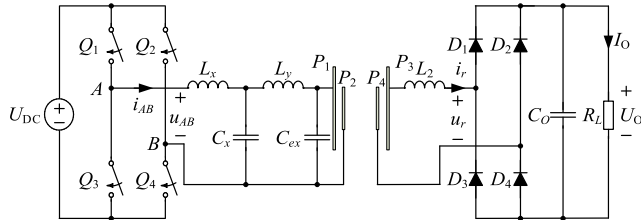| Misalignment	C_M	$C_P - C_M$	$C_S - C_M$
0 mm	71 pF	378 pF	379 pF
15 mm	65 pF	383 pF	384 pF
30 mm	57 pF	389 pF	389 pF
45 mm	48 pF	396 pF	395 pF
60 mm	40 pF	401 pF	402 pF
75 mm	32 pF	406 pF	407 pF

FIGURE 8. The proposed CPT system with high misalignment tolerance.

of u_{AB} is given as

$$u_{in}(t) = \frac{4U_{DC}}{\pi} \sin \frac{\pi D}{2} \sin \omega_1 t \qquad (11)$$

where D is the duty cycle of u_{in} in half cycle.

The output currents I_O and I_{Omis} are expressed as

$$I_O = \frac{2}{\pi} I_r \text{ and } I_{Omis} = \frac{2}{\pi} I_{rmis} \qquad (12)$$

To realize high performance of anti-misalignment, the gap between $\mathbf{I}_{rmis}$ and $\mathbf{I}_r$ should be narrowed. According to (9), the output current is designed as $I_{rmis}/I_r = I_{Omis}/I_O = 1$ and it could be simplified as

$$\left| \frac{t_1}{1 + \left(j\omega C_B' + t_1\right)\left(j\omega L_{11} + \frac{1}{j\omega C_A'}\right)} \right| - \omega C_B = 0 \qquad (13)$$

The value of C_M, C_P, C_S, C_M', C_P', and C_S' are determined by the structure of the capacitive coupler. Thus, according to (1) and (3), parameters C_A, C_B, C_C, C_A', C_B', C_C', L_1, and L_2 are only related to C_{ex}. According to (9), (10) and (13), the input impendence and the output current are only influenced by C_{ex} and L_{11}. Thus, with the required input impendence angle and the output current, C_{ex} and L_{11} can be determined by equations (10) and (13).

With (7), the capacitor C_x can be expressed as

$$C_x = \frac{L_{11} - L_1}{\omega^2 L_x (L_{11} + L_x - L_1)} \qquad (14)$$

Submitting (14) into (8), the inductor L_x is expressed as

$$L_x = \frac{\omega C_x U_{in} (L_{11} - L_1)}{I_r - \omega C_B U_{in}} \qquad (15)$$

The inductor L_y is calculated by (5). Until now, all compensation parameters L_x, L_y, C_x, C_{ex}, and L_2 are determined.

IV. EXPERIMENT VERIFICATION

To verify the above analysis and exhibit high anti-misalignment performance of the proposed CPT circuit, the proposed CPT prototype and the double-sided LC-compensated CPT prototype are built to provide the constant current of 2 A and the maximum transferred power of 120 W. The input voltage is 48V. The structure and size of the capacitive coupler is shown in Figure 7 and TABLE 1. The prototype of the proposed LCLC-L-compensated CPT circuit is shown in Figure 9. In this experiment, the equivalent capacitances C_M, $C_S - C_M$, and $C_P - C_M$ of the coupler without misalignment and with the 75 mm misalignment are taken as examples to verify the proposed CPT system. The input DC voltage is 48 V. The maximum equivalent resistance of the load is 30 Ω. The frequency f is designed as 500 kHz to reduce the system volume. Microcontroller TMS320F28335 is used to drive $Q_{1,2,3,4}$. SiC MOSFETs IMW120R045M1 are selected to construct the inverter. SiC diodes IDW30G65C5 are adopted to realize rectification. To avoid the breakdown of capacitors, several capacitors are connected in series and parallel.
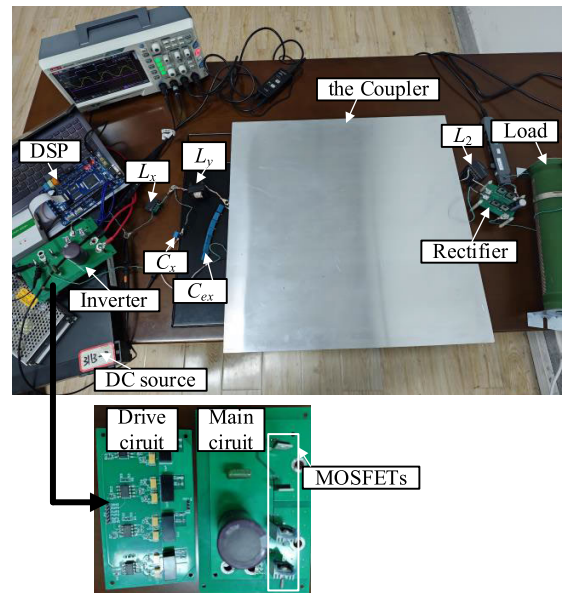

FIGURE 9. The prototype of the proposed CPT system.

Submitting $I_r = 2$ A, $C_M = 71$ pF, $C_P - C_M = 378$ pF, $C_S - C_M = 379$ pF, $f = 500$ kHz, (1), (3), and (4) into (10) and (13), parameters C_{ex} and L_{11} are calculated where the ZVS of MOSFETs and nearly input ZPA are all guaranteed. With (15), the inductance L_x is derived. Parameters C_x, L_2, and L_y are obtained by (14), (3), and (5) respectively. The compensation parameters of the double-sided LC-compensated CPT circuit and the pro-posed CPT circuit are given in Table 2. Circuit 1 and circuit 2 correspond to the double-sided LC-compensated CPT circuit and the proposed CPT circuit respectively.

As analyzed in [27], the double-sided LC-compensated CPT circuit can realize load-independent CC output and

TABLE 2. Compensation parameters for the double-sided LC-compensated CPT circuit and the proposed CPT circuit.

Parameters	Circuit 1	Circuit 2
C_x	/	2.21 nF
L_x	/	8.6 µH
L_y	/	37.7 µH
L_1	94.21 µH	/
L_2	94.21 µH	227 µH
C_{ex1}	632 pF	2.16 nF
C_{ex2}	632 pF	/

(a) $R_L = 15\ \Omega$

(b) $R_L = 30\ \Omega$

FIGURE 10. Experimental waveforms u_{GS}, u_{AB}, i_{IN}, and I_O of the proposed CPT circuit.
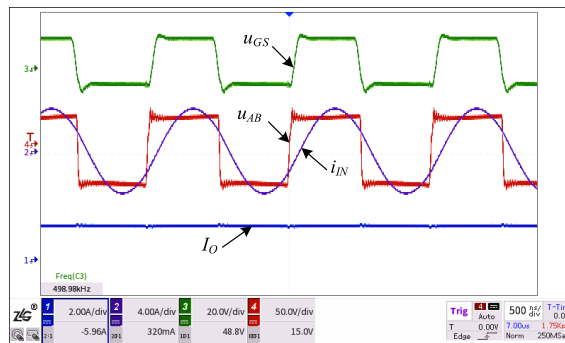

FIGURE 11. Experimental waveforms u_{GS}, u_{AB}, i_{IN}, and I_O of the double-sided LC-compensated CPT circuit at full load $R_L = 30\ \Omega$.

FIGURE 12. Experimental waveforms u_{GS}, u_{AB}, i_{IN} and I_O of the proposed CPT circuit under coupler misalignments.

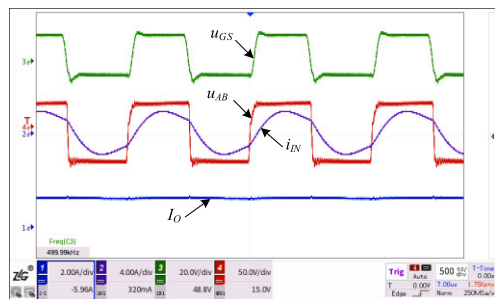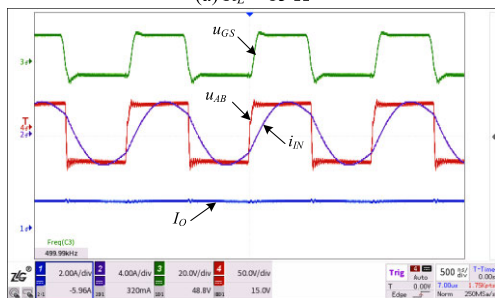**FIGURE 13.** The output currents based on different compensation circuits and misalignments.

input ZPA. The experimental waveforms u_{GS}, u_{AB}, i_{IN}, and I_O of the double-sided LC-compensated CPT circuit at full load $R_L = 30\ \Omega$ is shown in Figure 11. The nearly input ZPA, the soft-switching of MOSFET, and the constant output current of 2A are all realized.

Figure 12 shows experimental waveforms u_{GS}, u_{AB}, i_{IN}, and I_O of the proposed CPT circuit under coupler misalignments. When the distant of the coupler misalignment is 75 mm, the output current I_O is basically remained unchanged which is still around 2 A. Thus, the proposed LCLC-L-compensated CPT circuit has high performance of anti-misalignment.

To further demonstrate the superiority of the proposed CPT circuit, the output currents of the double-sided LC-compensated CPT circuit and the proposed CPT circuit with different distant of the coupler misalignment are shown in Figure 13. The output current of the double-sided LC-compensated CPT circuit corresponds to the unoptimized curve and the output current of the proposed CPT circuit
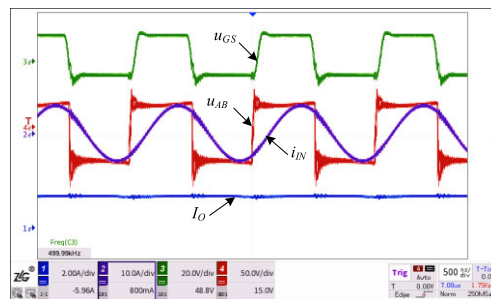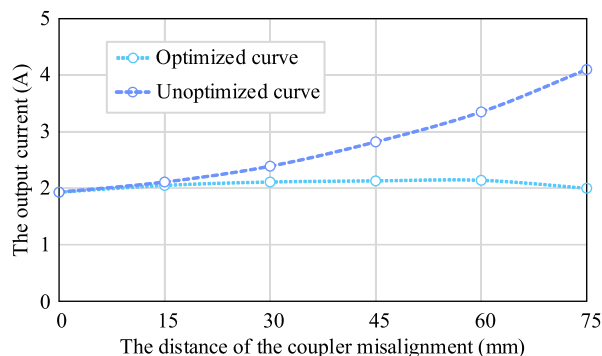
corresponds to the optimized curve. According to TABLE 1, when the misalignment happens, C_M decreases while $C_P - C_M$ and $C_S - C_M$ increase. Besides, equation (3) and (8) are not applicable, and the output currents of the double-sided LC-compensated CPT circuit and the proposed CPT circuit follow (2) and (9) respectively. By substituting the values of L_1, L_2, and equivalent capacitances from TABLE 1 into (2), as well as the values of L_{11}, L_2, and equivalent capacitances from TABLE 1 into (9), the output currents could be drawn as Figure 4. If the compensation inductance is L_1, the output currents of the double-sided LC-compensated CPT circuit under different misalignments are circled in red. If the

TABLE 3. Compensation for recent CPT systems and this work.

Reference	Environment	No. of plates	No. of compensation components	Misalignment	Control	ΔC_M	ΔP_{out} or ΔI_{out}	η
[4]	underwater	6	2 capacitors+2 transformers	9.4%	Unused	12.2 %	18%(P_{out})	84.3%
[27]	air	4	4 or 6	15.6%	Unused	/	50%(I_{out})	/
[28]	air	4	6 capacitors/ inductors+ Buck and Boost converters	45%	Used	/	0%(P_{out})	75%
[30]	air	4	4 capacitors/ inductors + 1 transformer	45%	Used	29.5%	8.3%(P_{out})	88.29%
This work	air	4	5	15%	Unused	55%	6%(I_{out})	86%

compensation inductance is L_{11}, the output currents of the proposed CPT circuit are circled in purple. To sum up, we can draw the conclusion that as the distance of the coupler misalignment increases, the output current of the double-sided LC-compensated CPT circuit changes dramatically, which would reduce the lifetime of the load and even make circuits overheat or burn, and the output current of the proposed CPT circuit is basically constant. Figure 13 provides further evidence for the analysis mentioned earlier and is consistent with the findings presented in Figure 4. Therefore, unlike the unoptimized curve, the proposed CPT circuit possesses high performance of anti-misalignment.

The maximum efficiency of the proposed CPT converter is measured around 89 % and the efficiency under misalignment condition is around 86 %. The losses are mainly distributed in the coupler plates, magnetic inductors, and rectifier diodes, which is not the key and omitted in this paper.

Table 3 shows the comparison between this work and the previous studies. As mentioned in Introduction and shown in [27], when significant misalignments occur, the equivalent capacitances of the CPT couplers would also undergo dramatic changes. Besides, several researches use complex control strategies or hybrid power transfer systems to improve the anti-misalignment performance. For this work, no control strategy is needed and the structures of the CPT coupler and the compensation network are all relatively simple. Furthermore, the maximum variation of the output current is 6% even if C_M changes dramatically (55%), indicating that the output current remains constant.

V. CONCLUSION

Inspired by the double-sided LC-compensated CPT circuit, this paper proposes an LCLC-L-compensated CPT system. After a systematic analysis, one load-independent constant current (CC) frequency with the nearly input zero-phase angle (ZPA) are derived. A parameter design method is also proposed in this paper to reduce the influence of the coupler misalignment and realize the soft-switching of MOSFETs. To demonstrate the superiority of the proposed CPT circuit,

the double-sided LC-compensated CPT prototype and the proposed CPT prototype are all built. Experimental results have validated the theoretical analysis well and the output current of the proposed CPT circuit is basically impregnable even though the coupler has a relatively large misalignment. Thus, without complex control strategy, the double-sided LCLC-L-compensated CPT circuit possesses high performance of anti-misalignment.

REFERENCES

[1] A. N. M. S. Hossain, P. Mohseni, and H. M. Lavasani, "Design and optimization of capacitive links for wireless power transfer to biomedical implants," *IEEE Trans. Biomed. Circuits Syst.*, vol. 16, no. 6, pp. 1299–1312, Dec. 2022.

[2] R. Sedehi, D. Budgett, J. Jiang, X. Ziyi, X. Dai, A. P. Hu, and D. McCormick, "A wireless power method for deeply implanted biomedical devices via capacitively coupled conductive power transfer," *IEEE Trans. Power Electron.*, vol. 36, no. 2, pp. 1870–1882, Feb. 2021.

[3] L. Yang, Y. Zhang, X. Li, B. Feng, X. Chen, J. Huang, T. Yang, D. Zhu, A. Zhang, and X. Tong, "Comparison survey of effects of hull on AUVs for underwater capacitive wireless power transfer system and underwater inductive wireless power transfer system," *IEEE Access*, vol. 10, pp. 125401–125410, 2022.

[4] E. Rong, P. Sun, K. Qiao, X. Zhang, G. Yang, and X. Wu, "Six-plate and hybrid-dielectric capacitive coupler for underwater wireless power transfer," *IEEE Trans. Power Electron.*, vol. 39, no. 2, pp. 2867–2881, Feb. 2024.

[5] D. Vincent, A. Praneeth, and S. S. Williamson, "Feasibility analysis of a reduced capacitive wireless power transfer system model for transportation electrification applications," *IEEE J. Emerg. Sel. Topics Ind. Electron.*, vol. 3, no. 3, pp. 474–481, Jul. 2022.

[6] V.-B. Vu, M. Dahidah, V. Pickert, and V.-T. Phan, "An improved LCL-L compensation topology for capacitive power transfer in electric vehicle charging," *IEEE Access*, vol. 8, pp. 27757–27768, 2020.

[7] Y. Wang, H. Zhang, and F. Lu, "3.5-kW 94.2% DC–DC efficiency capacitive power transfer with zero reactive power circulating," *IEEE Trans. Power Electron.*, vol. 38, no. 2, pp. 1479–1484, Feb. 2023.

[8] W. Gu, D. Qiu, X. Shu, B. Zhang, W. Xiao, and Y. Chen, "A constant output capacitive wireless power transfer system based on parity-time symmetric," *IEEE Trans. Circuits Syst. II, Exp. Briefs*, vol. 70, no. 7, pp. 2585–2589, Jul. 2023.

[9] S. Zang, Q. Zhu, L. Zhao, and A. P. Hu, "Capacitive power transfer system with integrated wide bandwidth communication," *IEEE Trans. Power Electron.*, vol. 37, no. 8, pp. 8805–8810, Aug. 2022.

[10] H. Zhang, F. Lu, H. Hofmann, W. Liu, and C. C. Mi, "A four-plate compact capacitive coupler design and LCL-compensated topology for capacitive power transfer in electric vehicle charging application," *IEEE Trans. Power Electron.*, vol. 31, no. 12, pp. 8541–8551, Dec. 2016.

[11] C. Cheng, F. Lu, Z. Zhou, W. Li, C. Zhu, Z. Deng, X. Chen, and C. Mi, "A multiload inductive power transfer repeater system with constant load current characteristics," *IEEE J. Emerg. Sel. Topics Power Electron.*, vol. 8, no. 4, pp. 3533–3541, Dec. 2020.

[12] J. Liu, C. S. Wong, C. Sun, F. Xu, X. Jiang, and K. H. Loo, "Software-reconfigurable multistage constant current wireless battery charging based on multiharmonic power transmission," *IEEE Trans. Power Electron.*, vol. 38, no. 4, pp. 5586–5597, Apr. 2023.

[13] Y. Liu, C. Liu, R. Huang, and Z. Song, "Primary multi-frequency constant-current compensation for one-to-multiple wireless power transfer," *IEEE Trans. Circuits Syst. II Exp. Briefs*, vol. 70, no. 6, pp. 2201–2205, Jun. 2023.

[14] B. Luo, R. Mai, L. Guo, D. Wu, and Z. He, "LC–CLC compensation topology for capacitive power transfer system to improve misalignment performance," *IET Power Electron.*, vol. 12, no. 10, pp. 2626–2633, Aug. 2019.

[15] D. Guo, Y. Su, H. Yin, H. Lan, and D. Li, "Self-adaptive resonance technology for wireless power transfer systems to eliminate impedance mismatches," *IEEE Trans. Power Electron.*, early access, pp. 1–14, Apr. 2023, doi: 10.1109/TPEL.2023.3265422.

[16] H. T. Nguyen, J. Y. Alsawalhi, K. A. Hosani, A. S. Al-Sumaiti, K. A. A. Jaafari, Y.-J. Byon, and M. S. E. Moursi, "Review map of comparative designs for wireless high-power transfer systems in EV applications: Maximum efficiency, ZPA, and CC/CV modes at fixed resonance frequency independent from coupling coefficient," *IEEE Trans. Power Electron.*, vol. 37, no. 4, pp. 4857–4876, Apr. 2022.

[17] J. Jiang, X. Dai, and A. P. Hu, "A dynamic tuning method for ZPA frequency operation of MEU-WPT system by DC input voltages regulation," *IEEE Trans. Power Electron.*, vol. 37, no. 9, pp. 11369–11381, Sep. 2022.

[18] X. Qu, H. Chu, Z. Huang, S.-C. Wong, C. K. Tse, C. C. Mi, and X. Chen, "Wide design range of constant output current using double-sided LC compensation circuits for inductive-power-transfer applications," *IEEE Trans. Power Electron.*, vol. 34, no. 3, pp. 2364–2374, Mar. 2019.

[19] X. Qu, H. Chu, S.-C. Wong, and C. K. Tse, "An IPT battery charger with near unity power factor and load-independent constant output combating design constraints of input voltage and transformer parameters," *IEEE Trans. Power Electron.*, vol. 34, no. 8, pp. 7719–7727, Aug. 2019.

[20] J. Rahulkumar., R. Narayanamoorthi., P. Vishnuram, M. Bajaj, V. Blazek, L. Prokop, and S. Misak, "An empirical survey on wireless inductive power pad and resonant magnetic field coupling for in-motion EV charging system," *IEEE Access*, vol. 11, pp. 4660–4693, 2023.

[21] J. Rahulkumar, R. Narayanamoorthi, P. Vishnuram, C. Balaji, T. Gono, T. Dockal, R. Gono, and P. Krejci, "A review on resonant inductive coupling pad design for wireless electric vehicle charging application," *Energy Rep.*, vol. 10, pp. 2047–2079, Nov. 2023.

[22] J. Rahulkumar, R. Narayanamoorthi, C. Balaji, and A. Savio, "A review on resonant inductive coupling pad design for wireless electric vehicle charging application," in *Proc. IEEE Transp. Electrific. Conf. Expo.*, Dec. 2023, pp. 1–8.

[23] J. Rahulkumar and R. Narayanamoorthi, "Power control and efficiency enhancement topology for dual receiver wireless power transfer EV quasi-dynamic charging," in *Proc. IEEE Transp. Electrific. Conf. Expo. (ITEC)*, Dec. 2023, pp. 1–6.

[24] Y. Hou, S. Sinha, and K. Afridi, "Tunable multistage matching network for capacitive wireless power transfer system," in *Proc. IEEE Wireless Power Transf. Conf. (WPTC)*, Jun. 2021, pp. 1–4.

[25] C. Liu, A. P. Hu, B. Wang, and N. C. Nair, "A capacitively coupled contactless matrix charging platform with soft switched transformer control," *IEEE Trans. Ind. Electron.*, vol. 60, no. 1, pp. 249–260, Jan. 2013.

[26] J.-Q. Zhu, Y.-L. Ban, Y. Zhang, C. Cheng, Z. Yan, R.-M. Xu, and C. C. Mi, "A novel capacitive coupler array with free-positioning feature for mobile tablet applications," *IEEE Trans. Power Electron.*, vol. 34, no. 7, pp. 6014–6019, Jul. 2019.

[27] S. Wang, Y. Yin, R. He, J. Liang, and M. Fu, "High-order compensated capacitive power transfer systems with misalignment insensitive resonance," *IEEE Trans. Circuits Syst. I, Reg. Papers*, vol. 69, no. 8, pp. 3450–3460, Aug. 2022.

[28] S. Sinha, A. Kumar, B. Regensburger, and K. K. Afridi, "Active variable reactance rectifier—A new approach to compensating for coupling variations in wireless power transfer systems," *IEEE J. Emerg. Sel. Topics Power Electron.*, vol. 8, no. 3, pp. 2022–2040, Sep. 2020.

[29] X. Qing, Y. Su, A. P. Hu, X. Dai, and Z. Liu, "Dual-loop control method for CPT system under coupling misalignments and load variations," *IEEE J. Emerg. Sel. Topics Power Electron.*, vol. 10, no. 4, pp. 4902–4912, Aug. 2022.

[30] B. Luo, T. Long, L. Guo, R. Dai, R. Mai, and Z. He, "Analysis and design of inductive and capacitive hybrid wireless power transfer system for railway application," *IEEE Trans. Ind. Appl.*, vol. 56, no. 3, pp. 3034–3042, May 2020.

[31] X. Qing, Z. Li, X. Wu, Z. Liu, L. Zhao, and Y. Su, "A hybrid wireless power transfer system with constant and enhanced current output against load variation and coupling misalignment," *IEEE Trans. Power Electron.*, vol. 38, no. 10, pp. 13219–13230, Oct. 2023.

[32] C. Cai, X. Liu, S. Wu, X. Chen, W. Chai, and S. Yang, "A misalignment tolerance and lightweight wireless charging system via reconfigurable capacitive coupling for unmanned aerial vehicle applications," *IEEE Trans. Power Electron.*, vol. 38, no. 1, pp. 22–26, Jan. 2023.

[33] H. Yuan, C. Liang, R. Zhang, Z. Ruan, Z. Zhou, A. Yang, X. Wang, and M. Rong, "A novel anti-offset interdigital electrode capacitive coupler for mobile desktop charging," *IEEE Trans. Power Electron.*, vol. 38, no. 3, pp. 4140–4151, Mar. 2023.

[34] C. Jiang, B. Wei, C. Xu, X. Wu, and H. He, "Efficiency improvement under coupler misalignment for dual-transmitter and single-receiver capacitive power transfer system," *IEEE Trans. Power Electron.*, vol. 38, no. 12, pp. 14872–14883, Dec. 2023.

[35] J. Lian and X. Qu, "Design of a double-sided LC compensated capacitive power transfer system with capacitor voltage stress optimization," *IEEE Trans. Circuits Syst. II, Exp. Briefs*, vol. 67, no. 4, pp. 715–719, Apr. 2020.

HUI DENG (Senior Member, IEEE) received the B.S. and M.S. degrees in computer science and technology from Fuzhou University, in 2006 and 2009, respectively. He is currently pursuing the Ph.D. degree with Tianjin University. From 2009 to 2019, he worked as a Senior Project Manager at Fujian Branch of China Telecom. He has been with Xiongan National Innovation Center Technology Company Ltd. His main research interests include wireless power transfer and intelligent transportation.

HUILIN GE received the B.S. and M.S. degrees in electrical engineering and the Ph.D. degree from Jiangsu University of Science and Technology, in 2023. He is currently an Associate Professor with the School of Automation, Jiangsu University of Science and Technology. His main research interest includes wireless power transfer.

JING LIAN received the B.S. degree in electrical engineering from China University of Mining and Technology in 2015, and the Ph.D. degree from Southeast University, in 2022. She is currently a Lecturer with the School of Automation, Nanjing University of Information Science and Technology. Her main research interest includes wireless power transfer.

• • •